ChemPubSoc Europe

DOI: 10.1002/batt.201900049

BATTERIES & SUPERCAPS
Articles

Creating Faradaic Carbon Nanotube Electrodes with Mild Chemical Oxidation

Robert K. Emmett,[a] Michael J. Kowalske[+],[a] Hansen Mou[+],[a] Mikaela Grady,[a] Han Jiang,[b] and Mark E. Roberts*[a]

The development of new materials to improve interfacial charge transfer characteristics will drastically improve energy storage, heterogeneous catalysis, and many other electrochemical applications. Here, we report a simple procedure that can harness the Faradaic nature of residual iron nanoparticle catalysts that endure within multi-walled carbon nanotubes (MWNT) post-synthesis, thereby alleviating the challenges associated with forging hybrid nanocomposite electrodes. Non-purified MWNTs, undergo a chemical oxidation process in acidic conditions with $KMnO_4$ to partially "unzip" the MWNTs and expose the redox-active iron nanoparticles to the electrolyte. A stable redox peak associated with the $Fe^{2+/3+}$ transition is achieved during the MWNT oxidation process yielding a ~350% increase in capacitance (>300 F g^{-1}) relative to purified MWNT electrodes (70 F g^{-1}). While these materials solely may be pragmatic as energy storage electrodes, the integration of redox species within an inert carbon electrode will also provide new opportunities to accelerate heterogeneous charge transfer reactions.

1. Introduction

The increasing demand for energy, fuels, and commodity chemicals necessitates advances in heterogeneous charge transfer interfaces to enhance energy storage capabilities and liquid-solid catalysis.[1–3] Carbon nanotubes (CNTs) are utilized for energy storage electrodes and chemical catalysis because of their electrical conductivity, chemical and thermal stability in various media, high surface area, matted percolating network, metal binding affinity, and controllable porosity.[4–6] Adding Faradaic dopants to carbon electrodes enhances the energy density of capacitors and facilitates charge transfer in batteries to promote greater power densities.[7] Advanced interfaces for charge transfer will also be beneficial to heterogeneous catalysis, permitting cheaper materials to reduce costs, increase output, and for fuel cells drastically increase their power densities.

Electrochemical double layer capacitors (EDLCs) contain the superior power and conductive capabilities of capacitors but lack the energy densities required for future technologies.[8,9] EDLC's superior power densities are attributed to their physical ion adsorption to the surface and therefore is limited by specific surface area.[7,10,11] Even the most porous carbon materials cannot surpass the inherit theoretical capacitive limit of 150–200 F g^{-1}.[12,13] Surface area restrictions have constrained single-walled CNTs (SWNTs) to a specific capacitance of 180 F g^{-1} and multi-walled CNTs (MWNT) to 100 F g^{-1}.[14] Expansion in energy and power demands necessitates a further amelioration in specific capacity for these materials to be common in commercial cells.[14] Theoretical specific capacitance is limited by the CNTs charge storage mechanisms, which only are proficient of storing charge along the sidewalls and open ends of the nanotube.[15]

Improving the lower capacitance restrictions of CNT electronics has been a prevalent research effort focusing on adding Faradaic energy storage mechanisms to existing, high power, high conductivity behavior.[16,17] Metal oxides composites have been extensively investigated to progress specific capacitance by exploiting the oxides ability to create weak bonds with surface CNT ions thereby storing charge.[18–20] This stored charge permits metal oxide composite materials to reach 1200–2200 F g^{-1} for rutherfordium systems, although their storage is highly rate dependent and they degrade with electrochemical usage.[18] Cheaper alternatives to metal oxides include incorporating electrically conducting polymers into the carbon electrodes that are able to store Faradaic charge.[11] These materials do compete in maximum capacity with metal oxides but are able to reach ~400 F g^{-1} at an abbreviated cost and more consistent cycle life constituting them as viable for supercapacitor applications.[21]

Residual transition metal catalysts incorporated into the CNT synthesis mechanism provide an immense opportunity to boost electro-catalytic activity due to their inherited redox capabilities.[22] These dopants are inactive in CNT electrodes because they are blocked from the electrolyte by the graphitic layers of the MWNTs.[23] However, our previous work demonstrated if these MWNTs are activated by exposing the electrode

[a] R. K. Emmett, M. J. Kowalske,[+] H. Mou,[+] M. Grady, Dr. M. E. Roberts
Department of Chemical and Biomolecular Engineering,
Clemson University
127 Earle Hall, 206 S Palmetto Blvd,
Clemson, SC 29634, USA
E-mail: mrober9@clemson.edu
[b] Dr. H. Jiang
Department of Material Science and Engineering,
Clemson University
161 Sirrine Hall; 515 Calhoun Drive
Clemson, SC 29634, USA
[+] These authors contributed equally to this work.

to high voltage, oxygen bubbles will nucleate on the metal nanoparticles and cause the MWNTs to ruptures near the end caps.[24] This permits the electrochemical redox reactions of the metal nanoparticles to be harnessed revealing a specific capacitance of 290 $F g^{-1}$ or a 61% increase over their SWNT counterparts and exceeding the theoretical limits on MWNT supercapacitors. This technology would also exploit the metal catalysts from the MWNT synthesis, spawning the metal-MWNT composites for petrochemical hydrogenation reactions.[25,26] By utilizing the already integrated Faradaic materials from synthesis, MWNTs based catalysis would become simpler and more economical to produce than current methods carried out via electron-beam deposition or functionalization.[27]

In this article, we describe a method to oxidize MWNTs to expose the lingering catalysts from their synthesis (6–9 wt%), which creates redox-active iron nanoparticles within the MWNTs. Previously, we performed electrochemical methods to activate these MWNTs, which proved efficacious in opening the end caps and improving electrochemical performance; however, a solution method has advantages in scalability and uniformity.[24] MWNTs have been chemically oxidized using piranha solution, H_2O_2, $KMnO_4$, $HClO_4$, and O_3 to unzip their nanotube structures.[28][29] Examination of MWNTs after oxidization showed that $KMnO_4$ was ideal for opening near the end caps and preserving catalysts over other oxidants. However, $KMnO_4$ will leave MnO_2 residue that can diminish the electrical properties of the resulting electrodes. By optimizing the oxidative treatment, the end caps of the MWNTs can be fractured without leaving excess residue or damaging the rest of the CNT structure, thereby maximizing the electrical performance of the resulting electrodes. Once the nanoparticles have been chemically oxidized, a stable $Fe^{2+/3+}$ redox couple is established which adds Faradaic behavior to the MWNTs for increased specific capacitance and also promotes heterogeneous liquid-solid charge transfer reactions.

2. Results and Discussion

2.1. Carbon Nanotube Activation

Multi-walled carbon nanotubes (MWNTs) are oxidized in sulfuric acid and potassium permanganate at assorted concentrations, times, and temperatures. Oxidized nanotubes are then diluted in water and sonicated with a surfactant to disperse the MWNTs before filtration. The vacuum filtration, with nylon membranes, process creates a free-standing buckypaper that is flexible and mechanically robust resulting in films that can be transferred with tweezers, withstand mild pulling, and compression. These electrodes are dried overnight at 80 °C to remove any remaining water before experimentation.

Residual ferrous nanoparticles remaining from the chemical vapor deposition synthesis process of carbon nanotubes are located within the caps of the MWNTs.[24] To create an optimal material that is suitable for liquid-solid interfacial Faradaic reactions, the nanoparticles must be accessible to charge transfer with the electrolyte and the MWNTs must maintain a relatively high conductivity by limiting the disruption to the π-electron system. This process described here promotes enhancing the extrinsic pseudocapacitance of these 2D carbon nanomaterials and is part of a developing trend in energy storage.[30,31] Iron nanoparticles, once activated are located on the surface of these electrodes; therefore, pseudocapacitive charge storage is driven by surface controlled charge transfer.[31] The molecular level-controlled oxidization treatment causes the nanotubes to systematically unzip thereby exposing the nanoparticles to the electrolyte as reported by Rangel et al.[32] However, the potassium permanganate utilized as the oxidizing agent also favors the deposition of MnO_2 on to the MWNTs surface blocking sites for charge storage.[32] Although MnO_2 is electroactive, it is also an insulating ceramic material which inhibits interactions between the electrolyte and the electrodes, impedes electrical transport, and restricts charge transfer to/from the redox-active iron nanoparticles.[32] It is expected that the oxidation process must be well-controlled to balance electrolyte access to the active nanoparticles and electrical conductivity of the carbon nanotube electrode, while minimizing the adsorption of MnO_2.

TGA (Figure 1a) and EDXS (Table 1) illustrate the adsorption of MnO_2 over time as evidenced by the increase in Mn, O, and K when MWNTs are oxidized at 40 °C and 0.1 M $KMnO_4$. The EDXS results are shown in elemental percentage to show the general trend of how the composition of Mn, O, and K increase during the oxidation reaction, even though carbon and iron remain constant. MnO_2 is deposited during the oxidation reaction resulting in a ceramic material that extends outward like a stone across the MWNTs. Also, the adsorption causes the total mass per area of the electrodes to increase, which negatively affects the specific capacity of the nanotubes. Thus, an optimal reaction condition exists where the MWNTs are sufficiently oxidized to maximize the Faradic content of the iron nanoparticles, while limiting the formation of MnO_2 on the nanotubes. Studying the kinetics of the oxidation reaction by utilizing the integral method reveals a second order nature, which is verified by the oxidation mechanism.

The oxidation reaction in 2 M H_2SO_4 begins with MnO_4^- reacting with an interior double bond on the MWNT (Figure 2a).[32] This bond creates a manganate ester and lengthens the distance between the two carbon atoms by 0.3 Å breaking the double bond and stressing other double bonds adjacent to the broken double bond increasing the likelihood of another

Table 1. Electron dispersion X-ray spectroscopy of MWNT electrodes (total mass is for $d = 3.5$ cm electrode) at varying oxidation times and 0.1 M $KMnO_4$ and 40 °C.

EDX for varying KMnO4 treatment time (%)				
Element	0 min	2 min	10 min	30 min
Total mass	62.1 mg	66.8 mg	72.0 mg	86.0 mg
C	90.4	84	77.9	65.2
Mn	–	4.1	8.2	16.9
O	3.1	2.9	8.8	13.1
Fe	6	3.6	4.9	4.2
Si	0.5	0.1	0.1	0.2
K	–	trace	0.1	0.4

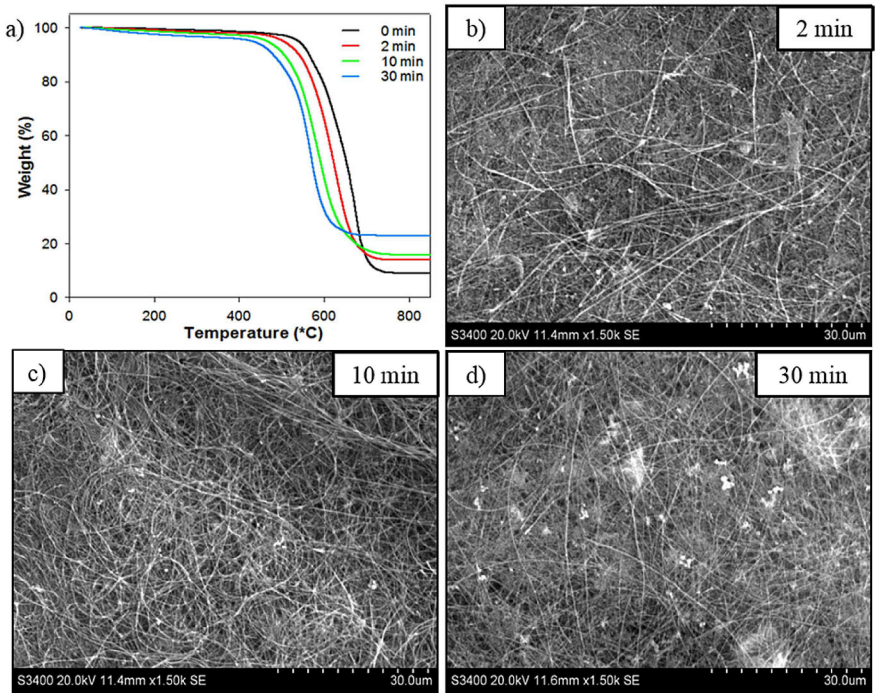

Figure 1. Physical characteristics of carbon nanotubes in different states of oxidation at 0.1 M $KMnO_4$ and 40 °C. Thermal gravitational analysis of fabricated electrodes at varying oxidation times (a). SEM images of the electrodes at 2 minutes (b), 10 minutes (c), and 30 minutes (d) of oxidation time.

MnO_4^- anion attacking these double bonds.[32] This stress promotes anions to attach to the tubes longitudinally down the MWNT.[32] Once these anions start to attach to sequential bonds on both sides of the initial site, the initial single bond breaks.[32] As this process works down the MWNT, the tubes "unzip" to expose the nanoparticles to the electrolyte (Figure 2a).[32] This verifies the 2nd order relationship we discovered in the adsorption because this "unzipping" reaction requires multiple manganate esters and is also autocatalytic due to the stress placed on adjacent bonds. The formation of MnO_2 adsorption pattern to the surface is verified through this mechanism. Fully reacted MWNTs contain the circular structure of the original MWNT's open end because these bonds are stronger than internal double bonds and would need excess oxidation to break. Due to adjacent double bonds being stressed and the agglomerating nature of MnO_2, the impervious MnO_2 surface grows outwards from the origin forming glassy stone shapes (Figure 1c,d & 2a).[32] The MnO_2 inhibits the MWNTs surface and therefore limiting its formation is important to maximize electrochemical performance. Unfortunately, a concentrated hydrochloric acid wash was attempted to remove the MnO_2 that adsorbs to the exterior but contained the negative externality of removing the iron nanoparticle catalysts. In addition to showing how the mass composition changes with $KMnO_4$ oxidation, TGA data also reveals that the carbon burn off temperature decreases with increasing oxidation time (Figure 1a). This is expected because the oxidation of the MWNTs weakens the average strength of the carbon bonds within the nanotubes and the annexation of MnO_2 cleaves the carbon nanotubes making them more susceptible to thermal decomposition.

SEM images of the MWNT electrodes at varying reaction times reveal the increasing extent of oxidation and the appearance of MnO_2 when reacted at 0.1 M $KMnO_4$ at 40 °C (Figure 1b,c,d). Figure 1d shows that after 30 minutes of oxidative time, many metallic agglomerates are dispersed throughout the electrode. Although MnO_2 is often used in supercapacitors its presence hinders electrochemical performance because it spawns a ceramic surface covering the MWNTs and ferrocene nanoparticles preventing electrolyte passage to the electrode. Excessive oxidation also disrupts the conductive structure of the MWNTs.

2.2. Electrochemical Performance

Electrochemical measurements were conducted with a Princeton VersaStudio potentiostat with an Ag/AgCl reference electrode, platinum mesh counter electrode, carbon nanotube working electrode, titanium current collector, and 0.5 M H_2SO_4 electrolyte. The electrode area for analysis was 0.5 cm^2, with masses in the range of 3.5 and 4.5 mg per 0.5 cm^2 and a thickness of approximately 340 μm. To stabilize and condition the electrode, cyclic voltammetry (CV) tests were run from 0 to 0.8 V (vs. Ag/Ag^+) for 20 cycles. CVs at various scan rates were then performed over the same voltage range to identify the scan rate dependence, calculate electrode capacitance, and determine the voltage efficiency of the electrodes. Electrochemical Impedance Spectroscopy (EIS) was conducted at 0.5 V to analyze the charge transfer resistances of the electrode at to the iron redox potential from 1 Hz to 100,000 Hz. Galvanostatic charge/discharge (GCD) experiments were conducted to ana-

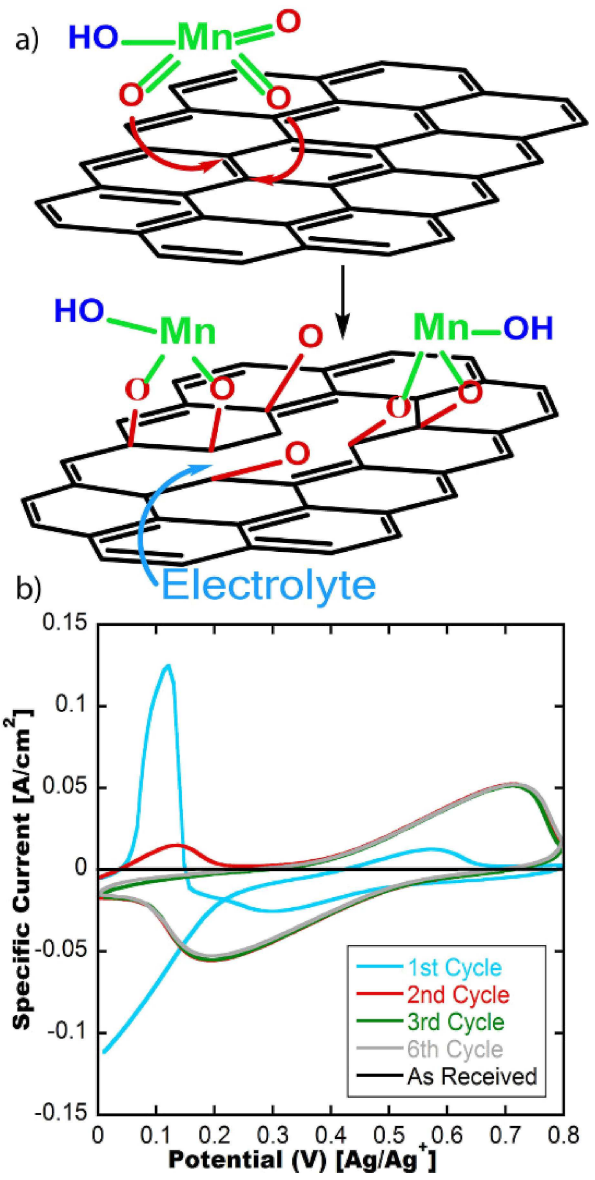

Figure 2. Activation of iron-containing CNTs schematic and stabilization by cyclic voltammetry at 100 mV s^{-1} in 0.5 M H_2SO_4. (a) Reaction schematic of KMnO4 partially opening the graphitic planes of the CNTs.[32] (b) Cyclic voltammetry of chemically activated carbon nanotube electrodes at 0.1 M $KMnO_4$, 10 minutes, and 40 °C activation conditions. This figure shows the activation process of the iron nanoparticles.

lyze the Faradaic behavior of the electrodes and to calculate their specific capacities.

Once the electrodes have been dried overnight to remove the remaining water, they are weighed and then stabilized by cyclic voltammetry (CV) at 100 mV s^{-1}. $KMnO_4$ oxidation creates openings in the graphitic layers of the MWNTs and permits charge transfer interactions between nanoparticle catalysts and the electrolyte. As received MWNTs (black) are fabricated into electrodes in the same manner and produce little to no electrochemical behavior between 0 and 0.8 V (vs. Ag/Ag$^+$). The first 100 mV s^{-1} CV activation cycle (blue) in Figure 2b displays decent iron redox (~0.5 V vs. Ag/Ag$^+$) performance but on the reduction scan a large cathode spike occurs around 0.1 V (vs. Ag/Ag$^+$). This anodic spike occurs due to the rapid oxidation of iron nanoparticles able to charge transfer with the electrolyte and making them redox active. A small irreversible oxidation peak at 0.2 V (wrt Ag/Ag$^+$) occurs on the 2nd cycle (red) and completes the activation process. Due to high proton concentration, in the acidic electrolyte, this irreversible oxidation peak is only present for one CV cycle. After cycle 3 (green) the electrode is stable and able to be tested electrochemically in order to determine the performance of the electrode although more cycles are performed to ensure the electrode is stable. The broad peaks occurring on the 3rd and 6th cycles revealed in Figure 2b are associated with the iron nanoparticles transferring (donating/accepting) electrons near their redox potential of 0.5 V (vs. Ag/Ag$^+$) (Figure 2b).

Incorporating Faradaic dopants, in the form of iron nanoparticle catalysts, decreases the charge transfer resistance of the electrodes by lowering the activation energy required for electron transport and diminishing internal electrical resistance of the electrodes. Transition metal nanoparticles reduce these resistances because they contain faster charge transfer constants due to their stability at two different oxidation states. Iron's redox couple lies within the aqueous electrochemical potential window and has excess electrons in their 3 s & 4d orbitals making it a prime candidate for catalysis. Figure 3 displays the EIS behavior of the electrodes at varying $KMnO_4$ concentrations, reaction temperatures, and reaction times. From the Nyquist plots, assuming an equivalent Randle's circuit, charge transfer resistances can be calculated by taking the diameter of the hemisphere, after factoring out diffusion noise on the lower frequency side (right).[33] From all three Nyquist plots it is apparent that without activation these MWNTs would not be a viable option for charge transfer interfaces due to their large charge transfer resistances (Figure 3). The presence of activated iron nanoparticles adds Faradaic charge transfer elements to standard charge separation energy storage of capacitor systems and therefore facilitates charge movement.

Figure 3a reveals the impedance behavior of the electrodes at varying oxidation times at 40 °C and 0.1 M $KMnO_4$. Even two minutes of oxidation decreases the charge transfer resistance from 55.7 Ω to 6.33 Ω, although the charge transfer resistance of the electrode decreases with increasing reaction time until it reaches a minimum of 2.08 Ω around 10 minutes. Past 10 minutes of oxidation the electrode resistance increases to 3.77 Ω at 15 minutes and 3.97 Ω at 30 minutes. This implies that near maximum electrochemical performance of the iron nanoparticles occurs around 10 minutes and additional time allows for further MnO_2 growth and destruction of the nanotubes, which hinders the interfaces performance because MnO_2 block interactions between the solid/liquid interfaces and the oxidation process opens the nanotubes disturbing the π-electron movement.

Figure 3b gives an evaluation of the effect reaction temperature has on electron transfer interactions with a concentration of 0.1 M $KMnO_4$ and reaction times of 10 minutes. Charge transfer resistances of the three oxidation temperatures seem to be similar with 30 °C, 40 °C, and 45 °C having resistances of 1.33 Ω, 1.20 Ω, and 2.16 Ω respectively. It does appear that

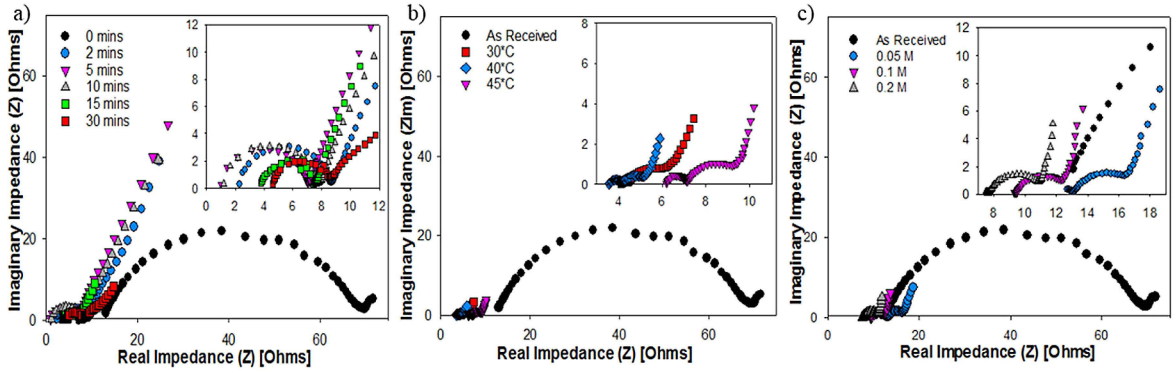

Figure 3. Electrochemical impedance spectroscopy of electrodes at various oxidizing conditions. (a) Nyquist curves of varying oxidative reaction times and a concentration of 0.1 M $KMnO_4$ and temperature of 40 °C. (b) Nyquist curves of varying oxidative reaction temperatures and at a concentration of 0.1 M $KMnO_4$ and 10 minutes reaction time. (c) Nyquist curves of varying $KMnO_4$ concentrations at a reaction time of 10 minutes and a temperature of 40 °C.

over-oxidation slightly occurs within the electrode at 45 °C, where an increase in resistance in observed. Figure 3c displays how electron transfer impedance within the electrode is affected by the concentration of $KMnO_4$ utilized at 40 °C and 10 minutes of reaction time. The charge transfer electrode resistances of 0.05 M, 0.1 M, and 0.2 M are 3.87 Ω, 1.93 Ω, and 3.07 Ω, respectively. Optimal performance, with respect to minimal charge transfer resistance, occurs at the 0.1 M concentration because the MWNTs are oxidized enough to expose the nanoparticles to the electrolyte without being over oxidized affecting the conductivity of the MWNTs. Concentration has a large effect of adsorption of MnO_2 which increases the "dead weight" of the electrode severely lowering specific capacity. Incorporating iron nanoparticles into the electrodes decreases the resistance of the electron transfer interactions, however, the quantity of MWNT oxidation is important for establishing an optimized electrode with minimal charge transfer resistances.

The further electrochemical analysis was conducted on the assorted oxidative conditions through CV at 10 $mV\,s^{-1}$ and GCD 4 $mA\,cm^{-2}$ analysis. Figure 4a shows the increased Faradaic performance of 10 min of oxidation reaction time at 40 °C and 0.1 M $KMnO_4$. Also, over-oxidation at 30 min is portrayed by the slanted profile of the CV curve due to the diffusion tails occurring near the potential limits of 0 and 0.8 V (vs. Ag/Ag^+). MWNTs oxidized for 2 min have limited efficacy due to a smaller concentration of activated iron nanoparticles. All three CVs curves (Figure 4a,b,c) demonstrate the performance of the untreated electrodes as inferior for energy storage applications as expected. Comparing the electrode performance at fluctuating oxidation reaction temperatures for 10 min reactions at 0.1 M illustrates the maximum capacity materializes when MWNTs are treated at 40 °C due to their higher redox current. An increase in reaction temperature up to 45 °C causes a reduction in specific capacitance due to the increased electrode mass resulting from MnO_2 formation. At an oxidation reaction time of 10 min, the CV behavior of MWNTs treated in 0.05 M, 0.1 M, and 0.2 M $KMnO_4$ solutions deviates significantly, with 0.1 M treated electrodes showing optimal redox behavior. When the oxidant reaction concentration is too low (0.05 M), MWNTs exhibit low voltage efficiency due to limited exposure of iron nanoparticles; however, at high reaction concentrations (0.2 M), MWNTs have an analogous voltage efficiency, but notably lower specific capacitance due to the enlarged mass affiliated with MnO_2 formation (Figure 4c).

A well understood trend of EDLCs is increasing specific surface area improves specific capacitance of the capacitor.[34] This occurs because the capacitors store energy by the physical separation of charge between the two electrodes; therefore, greater available area on the electrodes permits greater quantities of charge that can be stored on each electrode.[35] The activation process described in this paper causes cracks in the MWNTs which slightly increases the specific surface area, although these MWNTs are large ($d = 70$ nm) and have minimal EDLC behavior before activation. Therefore, the increase in electrochemical performance due to increased specific surface area is considered minimal. A larger concern to the EDLC behavior is the adsorption of MnO_2 which is also electrochemically active. Upon analyzing the CV curves in Figure 3a–c the predominant capacitance occurs from the bell-shaped peaks from the Faradaic charge transfer rather than the rectangular shape of EDLC energy storage. Also, analyzing Figure 3d–f we can easily understand that $>90\%$ of the specific capacity occurs due to Faradaic energy storage from the flat (slope approaching 0) discharge region containing most of the specific capacity.

GCD data shown in Figure 4d shows complementary conclusions as the CV data, in that MWNTs oxidized for 10 min display the highest specific capacity and "as received" MWNTs exhibit extremely weak performance. MWNTs reacted for 15 and 30 min, at 40 °C and 0.1 M, have reduced capacitance values due to blockage of the MWNTs and Faradaic nanoparticles by MnO_2. This is validated by the EIS contour delineated in Figure 3a, even though a decrease in discharge voltage is not substantial in the CV results (Figure 4a). GCD data reveals the effect of oxidation reaction temperature and that electrodes treated at 40 °C have superior charge transfer capabilities. This is confirmed because these electrodes exhibit elevated voltage efficiencies and specific capacities when

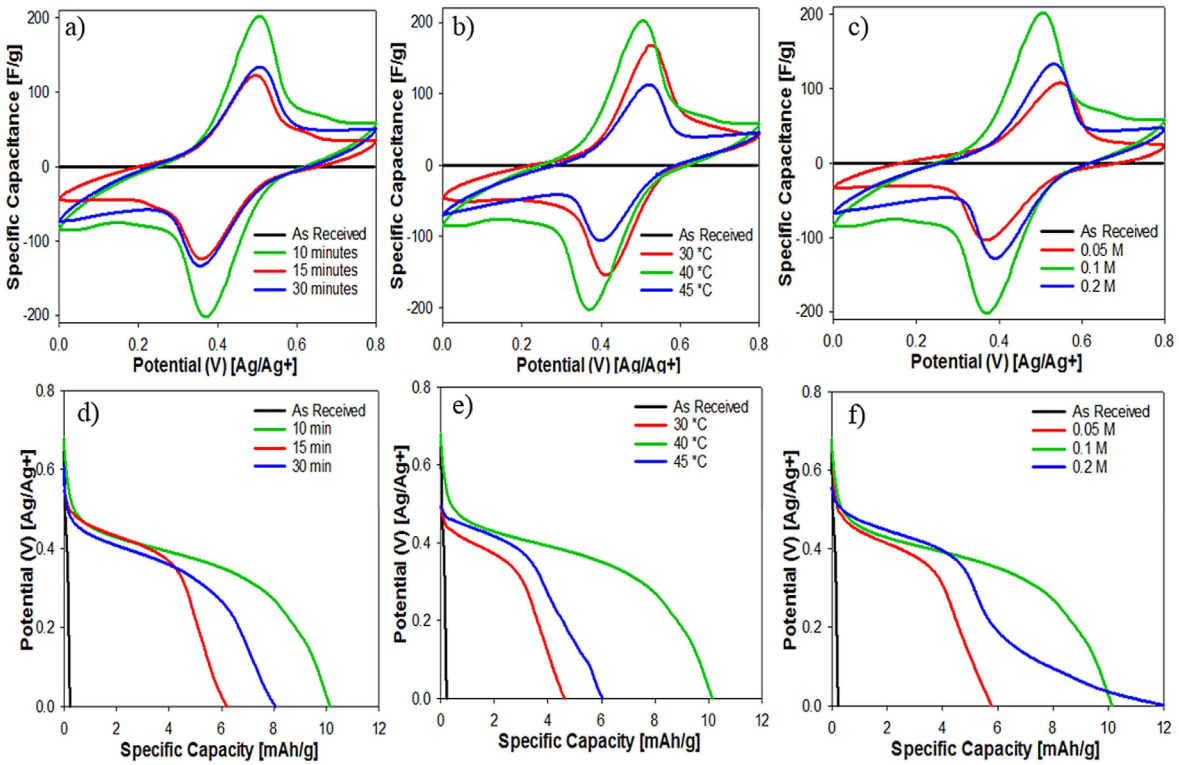

Figure 4. Electrochemical performance of chemically oxidized electrodes. (a) Normalized cyclic voltammetry (CV) curves at 10 mV s^{-1} of electrodes with different oxidative reaction times with a concentration of 0.1 M $KMnO_4$ and a temperature of 40 °C. (b) Normalized CV curves at 10 mV s^{-1} of varying reactive temperatures at an oxidative concentration of 0.1 M $KMnO_4$ and 10 minutes reaction time. (c) Normalized CV curves at 10 mV s^{-1} of variable $KMnO_4$ concentration at a reaction temperature of 40 °C and 10 minutes reaction time. (d) Galvanostatic discharge curves at 4 mA cm^{-2} of different oxidative reaction times with a concentration of 0.1 M KMnO4 and a temperature of 40 °C. (e) Galvanostatic discharge curves at 4 mA cm^{-2} of varying reactive temperatures at an oxidative concentration of 0.1 M $KMnO_4$ and 10 minutes reaction time. (f) Galvanostatic discharge curves at 4 mA cm^{-2} of variable $KMnO_4$ concentration at a reaction temperature of 40 °C and 10 minutes reaction time.

compared to electrodes with higher or lower oxidation temperatures (Figure 4e).

A slight bump is exhibited by the "as received" (untreated) electrodes near the oxidation potential of ferrocene and is attributed to a small amount of residual iron catalyst within the electrodes. Scrutinizing the oxidation reaction concentration demonstrates an oxidation treatment of 0.1 M generates electrodes with the topmost Faradaic specific capacity (capacity above the drop-off voltage) but 0.2 M reactions contains the highest specific capacities due to longer low voltage discharge times. This is attributed to increasing adsorption of MnO_2, which has a capacitor-like discharge behavior, leading to the additional linear profile at low potentials not seen in other discharge curves. These capacities are not useful for battery/supercapacitor application because they deliver inferior power densities. Overall the GCD data agrees with the previously show CV and EIS data that the optimal electrochemical performance occurs under the oxidation reaction of 0.1 M $KMnO_4$, 10 minutes, and 40 °C.

2.3. Comparison of Electrochemical, $KMnO_4$ Activated Electrodes

MWNTs oxidized with the $KMnO_4$ illustrate increased specific capacitance in correlation to our previously published electrochemical activation mechanism,[24] as indicated by the expanded area under the CV curves in Figure 5a and the lengthened GCD curves in Figure 5b. This can be attributed to the $KMnO_4$ oxidation process that reacts on the MWNTs when they are dispersed in water preceding the electrode fabrication. Electrochemical activation ensues when the electrode is already synthesized, therefore; the $KMnO_4$ oxidant has admittance to all of the MWNTs to stimulate all the iron nanoparticles present in the nanotubes. Electrochemical oxidation exposes most of the nanoparticles from exterior MWNTs but cannot fissure all the nanotubes due to steric hindrances and inter-nanotube contact within a fully constructed buckypaper electrode. $KMnO_4$ treated MWNTs display a specific capacitance increase of 10.5% over electrochemically activated tubes, suggesting an increase in Faradaic activity. Furthermore, $KMnO_4$ activated MWNTs have 35.8% lower charge transfer resistance than the electrochemical treated MWNT electrodes (Figure 5c). This decreased charge transfer resistance is caused by the increase in Faradaic mediators, which increases the quantity of catalysts that diminish the energy required for electron transfer leading to

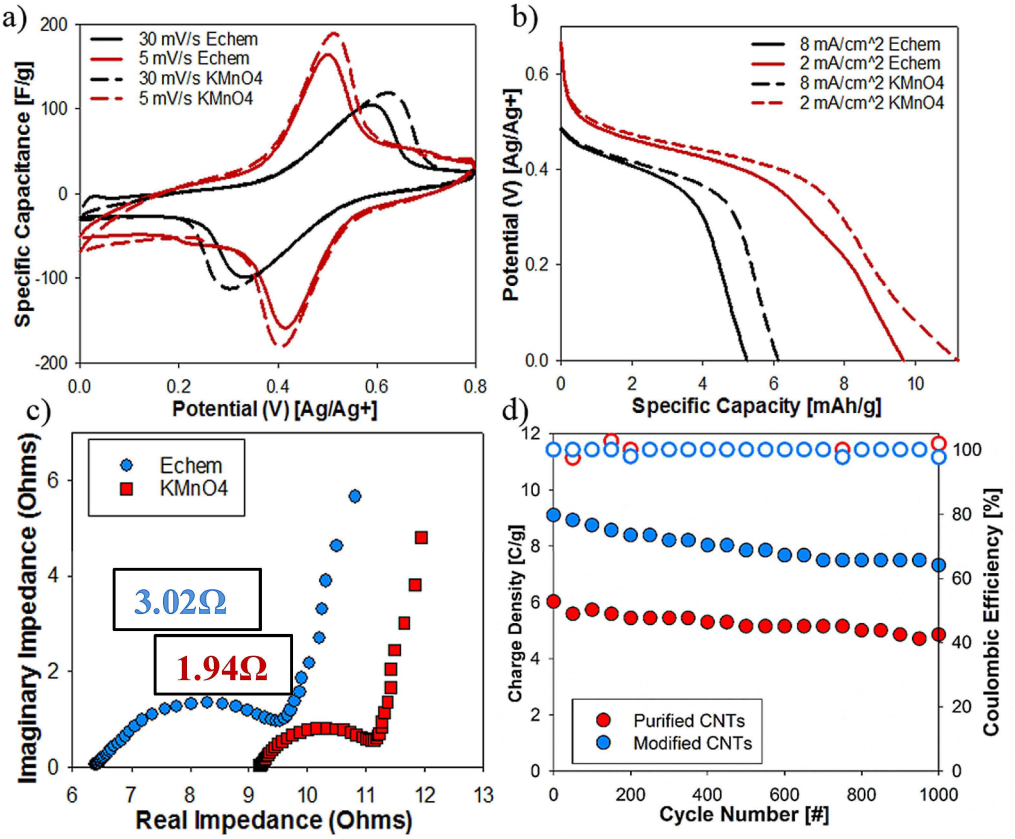

Figure 5. Electrochemical performance comparison of electrochemically and chemically activated electrodes. Chemically activated electrodes were activated at 0.1 M $KMnO_4$, 40 °C, and 10 minutes of reaction time. (a) Cyclic voltammetry at 30 mV s^{-1} (black) and 5 mV s^{-1} (red) comparing chemically oxidized electrodes (dashed lines) and electrochemically oxidized electrodes (solid lines). (b) Galvanostatic discharge curves at 8 mA cm^{-2} (black) and 2 mA cm^{-2} (red) of chemically oxidized electrodes (dashed lines) and electrochemically activated electrodes (solid lines). (c) Nyquist plot comparison of electrochemically activated electrodes (blue diamonds) and chemically activated electrodes (red squares). (d) Cycle life of modified (blue) and purified (red) CNT electrodes over 1000 cycles comparing the charge densities (filled symbols) and coulombic efficiencies (open symbols).

the increased performance in Figure 5a,b. GCD experiments in Figure 5b reveal a 16.5% increase in specific capacity at 4 mA cm^{-2} for $KMnO_4$ activated over electrochemically activated electrodes. $KMnO_4$ activation method occurs before the fabrication of the electrode and is a simple liquid phase reaction that can easily be scaled to operate at larger batch sizes or even be modified to a continuous system. The difficulty from large production would be the filtration step of the electrode fabrication, which could be conducted by gravity or reduced pressure filtration. Electrochemically activated MWNTs is un-scalable because only the tubes exposed to the electrical current are activated.

$KMnO_4$ activated electrodes exhibit a specific capacitance of 316 F g^{-1} or 2.16 F cm^{-2} at a scan rate of 3 mV s^{-1} with a 0.5 M H_2SO_4 electrolyte in our 3-electrodes setup when scanned from −0.4–1.3 V (vs. Ag/Ag$^+$).[24] Literature values of other carbon and metal oxide composites include MWNT/polypyrrole composites which have reached 170 F g^{-1} and MWNT/RuO_2 (1 wt%) composites containing specific capacitances of 80 F g^{-1}.[7] Graphene based metal oxide composites have reported large specific capacities of 479 F g^{-1} with RuO_2, 315 F g^{-1} with MnO_2, 250 F g^{-1} with nitrogen-doped carbon materials.[7,36] Materials reported here have the benefit of being cheaper than most CNTs due to their synthesis catalysts and the removal purification step. Also iron is a cheaper and more readily available transition metal dopant than many of the tradition transition metals used in pseudocapacitors. Our capacitances in aqueous conditions are greatly improved over other iron carbon composites which have been reported at 117–220 F g^{-1} and our materials are using the iron left behind in the carbon nanomaterials after synthesis.[36]

Long term stability of these supercapacitor devices were analyzed by repetitive GCD cycles from 1–0 V at 2 mA cm^{-2} for both modified and purified MWNT electrodes for 1000 cycles. From Figure 5d the coulombic efficiencies, over the 1000 cycles, were maintained at 100%, which is expected of capacitors. It is important to note that this is true with the iron-containing tubes even though they have a Faradaic element. Modified tubes have a ~50% increase in charge density over purified tubes, which has been established previously.[24] Iron-containing tubes maintain 82.4% of their initial capacity after 1000 cycles and pure CNT maintain 85.3% of their initial capacity (Figure 5d). Electrodes containing Faradaic iron nanoparticles only decrease their capacitive fade slightly, proving their superior charge densities are viable over the lifetime of the supercapacitor.

Literature values for capacity retention for metal oxide/carbon composites vary with how strong the interaction is between the transition metal and the carbon structure. MnO_2 carbon composites have reported 72% with mesoporous carbon, 93% with reduced graphene oxide, and 73% with carbon nanofibers for 1000 cycles.[36,37] Nickel, cobalt, and rutherfordium composites are consistently around 90% retention for 1000 cycles.[36–38] However when comparing to iron composites in literature, their retention rates over 1000 cycles in the literature are 73% with a sol-gel method, 60% with CNTs, and 99% with graphite foam-CNT composite. This establishes when comparing iron to iron our electrodes contain greater retention rates for similar simple composites.[37,39,40]

3. Conclusions

In summary, this work demonstrates a chemical oxidation process that unleashes the Faradaic nature of the residual iron catalyst remaining from MWNT synthesis to increase their specific capacitance beyond the EDLC limitations. By heating iron-containing MWNTs in acidic $KMnO_4$ solutions, the nanotubes were oxidized and unzipped to expose the iron nanoparticles for increased charge storage capacity via Faradaic reactions. The inclusion of stable redox-active iron nanoparticles results in a decrease in charge transfer resistances and an increase in specific capacitance from the Faradaic processes. The optimal oxidation conditions for iron-doped MWNTs occurred at 0.1 M $KMnO_4$, 40 °C, and 10 min treatment time, resulting in a specific capacitance of 316 $F g^{-1}$ (2.16 $F cm^{-2}$), which represents a significant improvement over untreated MWNTs. Oxidation conditions were optimized to limit MnO_2 growth while making all of the iron nanoparticles accessible to the electrolyte solution. Relative to the electrochemical activation process reported previously,[21] our $KMnO_4$ oxidation process results in MWNTs with a 16.5% increase in specific capacity. It is important to note that the chemical oxidation procedure has the additional benefit of being easily scalable for larger scale applications. Further improvements may be possible with an investigation into different CVD catalysts and SWNTs.

Experimental Section

Electrode Treatment and Fabrication

MWNT nanotubes (diameter = 70–80 nm, length = 10 μm) are used as received from NanoTech Labs. These MWNTs are synthesized by chemical vapor deposition with a ferrocene-xylene catalyst, where ~6–9% is iron catalysts and ~3–8% is amorphous carbon impurities. The MWNTs were submerged into 10 mL of 2 M sulfuric acid with varying concentrations of $KMnO_4$. The nanotubes are then heat treated at temperatures varying from 30–60 °C for reactions times between 2 and 60 minutes to oxidize and crack the nanotubes. These solutions are then diluted to 100 mL with 1.5 g sodium dodecyl sulfate and sonicated to disperse the CNTs. Vacuum filtration with a nylon membrane (0.47 μm) was performed to produce free-standing buckypaper electrodes that can be handled with tweezers, providing a convenient platform for electrochemical testing. These electrodes have a thickness of 340 μm ± 22 μm Electrodes are dried overnight in an oven at 80 °C to remove excess water. These electrodes were cut with scissors to be used in electrochemical testing with an active surface area of 0.5 cm^2.

Electrochemical Analysis

Electrochemical experiments were carried out using a Versastudio potentiostat for standard battery testing of cyclic voltammetry (CV, 0–0.8 V), galvanostatic charge/discharge (GCD, 0–0.8 V), and electrochemical impedance spectroscopy (EIS, 0.5 V) over a frequency range of 100,000–1 Hz. Electrodes were first stabilized by CV for 20 cycles from 0–0.8 V before electrochemical testing was conducted. The reference electrode was silver/silver chloride, the auxiliary electrode was a platinum mesh, and the current collector for the working electrode was titanium foil. All tests were conducted with 0.5 M H_2SO_4 as the electrolyte.

Physical Analysis

TGA (TA instruments Q-5000) analysis was conducted on finalized electrodes to determine the residual metal composition after chemical oxidation by heating the finished electrode in the presence of air up to 850 °C at a heating rate of 20 °C min^{-1}. Scanning Electron Microscopy (SEM) and Electron Dispersion X-ray Spectroscopy (EDXS) (HITACHI s-3400 N) were conducted, under full vacuum, to determine the structure of the post-oxidized nanotubes and to determine the elemental composition of the electrodes after oxidation.

Acknowledgements

The authors would like to acknowledge Kim Ivey for her assistance with the thermal gravitational analysis testing performed in the manuscript.

Conflict of Interest

The authors declare no conflict of interest.

Keywords: electrochemistry · heterogeneous catalysis · carbon nanotubes · supercapacitors · oxidation

[1] B. Dunn, B. Dunn, H. Kamath, J. Tarascon, *Sci. Mag.* **2011**, *334*, 928.
[2] M. M. Thackeray, C. Wolverton, E. D. Isaacs, *Energy Environ. Sci.* **2012**, *5*, 7854.
[3] S. Robert, *Angew. Chem. Int. Ed.* **2015**, *54*, 3465.
[4] K. Dae-Won, K. Ki-seok, P. Soo-Jin, *Carbon Lett.* **2012**, *13*, 157.
[5] Q. Yang, Z. Xu, C. Gao, *J. Energy Chem.* **2018**, *27*, 6.
[6] S. Chen, K. Li, J. Zhang, X. Liu, W. Pan, *J. Energy Chem.* **2018**, *0*, 1.
[7] A. González, E. Goikolea, J. Andoni, R. Mysyk, *Renewable Sustainable Energy Rev.* **2016**, *58*, 1189.
[8] A. Khaligh, Z. Li, *Veh. Technol. IEEE Trans.* **2010**, *59*, 2806.
[9] Y. Sun, Q. Wu, G. Shi, *Energy Environ. Sci.* **2011**, *4*, 1113.
[10] Y. Zhai, Y. Dou, D. Zhao, P. F. Fulvio, R. T. Mayes, S. Dai, *Adv. Mater.* **2011**, *23*, 4828.
[11] G. Wu, P. Tan, D. Wang, Z. Li, L. Peng, Y. Hu, C. Wang, W. Zhu, S. Chen, W. Chen, *Sci. Rep.* **2017**, *7*, 1.

[12] C. Merlet, B. Rotenberg, P. A. Madden, P.-L. Taberna, P. Simon, Y. Gogotsi, M. Salanne, *Nat. Mater.* **2012**, *11*, 306.
[13] A. Burke, *Electrochim. Acta* **2007**, *53*, 1083.
[14] M. Pumera, *Chem. Eur. J.* **2009**, *15*, 4970.
[15] W. Yuan, Y. Zhou, Y. Li, C. Li, H. Peng, J. Zhang, Z. Liu, L. Dai, G. Shi, *Sci. Rep.* **2013**, *3*, 1.
[16] S. S. Raut, B. R. Sankapal, M. S. A. Hossain, S. Pradhan, R. R. Salunkhe, Y. Yamauchi, *Eur. J. Inorg. Chem.* **2018**, *2018*, 137.
[17] W. Liu, Y. Tang, Z. Sun, S. Gao, J. Ma, L. Liu, *Carbon* **2017**, *115*, 754.
[18] M. Zhi, C. Xiang, J. Li, M. Li, N. Wu, *Nanoscale* **2013**, *5*, 72.
[19] K. Zhu, Y. Jin, F. Du, S. Gao, Z. Gao, X. Meng, G. Chen, Y. Wei, Y. Gao, *J. Energy Chem.* **2018**, *0*, 1.
[20] Y. Li, X. Han, T. Yi, Y. He, X. Li, *J. Energy Chem.* **2018**, *0*, 1.
[21] M. R. Arcila-Velez, R. K. Emmett, M. Karakaya, R. Podila, K. P. Díaz-Orellana, A. M. Rao, M. E. Roberts, *Synth. Met.* **2016**, *215*, 35.
[22] G. Lota, K. Fic, E. Frackowiak, *Energy Environ. Sci.* **2011**, *4*, 1592.
[23] H. Kim, M. J. Kaufman, W. M. Sigmund, D. Jacques, R. Andrews, *J. Mater. Res.* **2003**, *18*, 1104.
[24] R. K. Emmett, M. Karakaya, R. Podila, M. R. Arcila-Velez, J. Zhu, A. M. Rao, M. E. Roberts, *J. Phys. Chem. C* **2014**, *118*, 26498.
[25] P. S. Kumbhar, R. Dutartre, P. Geneste, P. Bernier, *J. Am. Chem. Soc.* **1994**, *116*, 7935.
[26] G. G. Wildgoose, C. E. Banks, R. G. Compton, *Small* **2006**, *2*, 182.
[27] N. Franklin, Y. Zhang, N. W. Franklin, R. J. Chen, H. Dai, *Chem. Phys. Lett.* **2000**, *331*, 35.
[28] K. C. Hwang, *J. Chem. Soc. Chem. Commun.* **1995**, *04*, 173.
[29] K. Hernadi, A. Siska, L. Thiên-Nga, L. Forró, I. Kiricsi, *Solid State Ionics* **2001**, *141–142*, 203.
[30] P. Nakhanivej, X. Yu, S. K. Park, S. Kim, J. Hong, H. J. Kim, W. Lee, J. Y. Hwang, J. E. Yang, C. Wolverton, J. Kong, M. Chhowalla, H. S. Park, *Nat. Mater.* **2019**, *18*, 156.
[31] X. Yu, S. Yun, J. S. Yeon, P. Bhattacharya, L. Wang, S. W. Lee, X. Hu, H. S. Park, *Adv. Energy Mater.* **2018**, *8*, 1.
[32] N. L. Rangel, J. C. Sotelo, J. M. Seminario, *J. Chem. Phys.* **2009**, *131*, 1.
[33] J.-M. Atebamba, J. Moskon, S. Pejovnik, M. Gaberscek, *J. Electrochem. Soc.* **2010**, *157*, A1218.
[34] Y. Zhang, H. Feng, X. Wu, L. Wang, A. Zhang, T. Xia, H. Dong, X. Li, L. Zhang, *Int. J. Hydrogen Energy* **2009**, *34*, 4889.
[35] R. A. Fisher, M. R. Watt, W. Jud Ready, *ECS J. Solid State Sci. Technol.* **2013**, *2*, M3170.
[36] A. Borenstein, O. Hanna, R. Attias, S. Luski, T. Brousse, D. Aurbach, *J. Mater. Chem. A* **2017**, *5*, 12653.
[37] V. C. Lokhande, A. C. Lokhande, C. D. Lokhande, J. H. Kim, T. Ji, *J. Alloys Compd.* **2016**, *682*, 381.
[38] W. Jiang, D. Yu, Q. Zhang, K. Goh, L. Wei, Y. Yong, R. Jiang, J. Wei, Y. Chen, *Adv. Funct. Mater.* **2015**, *25*, 1063.
[39] X. Cheng, X. Gui, Z. Lin, Y. Zheng, M. Liu, R. Zhan, Y. Zhu, Z. Tang, *J. Mater. Chem. A* **2015**, *3*, 20927.
[40] C. Guan, J. Liu, Y. Wang, L. Mao, Z. Fan, Z. Shen, H. Zhang, J. Wang, *ACS Nano* **2015**, *9*, 5198.

Manuscript received: March 26, 2019
Revised manuscript received: July 8, 2019
Accepted manuscript online: July 9, 2019
Version of record online: August 7, 2019